A combined experimental and numerical study of the behaviour of paperboard composites up to failure

Gabriella Bolzon *, Marco Talassi

Department of Civil and Environmental Engineering, Politecnico di Milano, Milano, Italy

1. Introduction

Commonly used packaging material consists of functionally layered composites combining paperboard plies (260–400 µm nominal thickness [1]), which confer stiffness and strength, with a thin aluminium foil (6–9 µm thickness), which contributes to the overall mechanical properties and acts as a barrier from external agents together with external coating layers made of polymeric films (15–30 µm thick). Components are produced in coils and are assembled together by the thermo-mechanical adhesion.

Paperboard presents markedly anisotropic mechanical properties, which are transferred to the overall composite. As an example, Fig. 1 visualizes the characteristic output of uniaxial tensile tests performed on two paperboard batches under displacement control (20 mm/min) according to Standard procedures [2]. Specimens consist of thin material strips (15 mm wide, 180 mm long) cut parallel to machine direction (MD or 0°), cross direction (CD or 90°) and diagonal (45°) direction. The graphs in Fig. 1 represent nominal stress versus nominal strain curves, which are quite repetitive and little dispersed. Typical features of the material response are high stiffness and strength along MD, while ductility (in the sense of large irreversible deformation before material failure) is exhibited along CD.

The stress–strain relationships are smoothly non-linear up to failure, induced by a macroscopic crack that suddenly crosses the specimen orthogonally to the loading direction. The unstable nature of the brittle fracture process concerning paper-based materials has been evidenced in a recent contribution [3], performing uniaxial tests along CD and MD. Controlled crack propagation was achieved only with specimens of unusual aspect ratio, namely strips two times wider than long. Still, a rather sharp stress drop-off was observed beyond the peak load.

Several elastic–plastic constitutive models of different complexity have been proposed to reproduce the continuum response of paper-based materials (e.g. [4–8]) while biaxial strength data reported in the literature ([9,10]) fed the formulation of several failure criteria. However, less attention has been usually paid to the failure modes, specifically considered in the present contribution.

Novel experimental results have been produced with the prototype instrumentation shown in Fig. 2, designed for inverse analysis purposes [11] and presented in an earlier version in [12]. The equipment is inspired by burst strength testers for paper [13] but additional information concerning the deformation of the material sample during the experiment is returned in digital format.

The considered testing procedure shares some similarities with the bubble inflation technique applied to polymeric membranes where, on the contrary of the present applications, large strains represent an issue but the expected material response is isotropic; see, e.g. [14] and the references listed therein.

Pressurized air contained in the vessel shown in Fig. 2 applies controlled uniform load to the surface of a foil placed over a circular opening and constrained by an airproof flange. During the test, a

* Corresponding author. Tel.: +39 02 2399 4319; fax: +39 02 2399 4300.
  E-mail address: gabriella.bolzon@polimi.it (G. Bolzon).

Fig. 3. Graphical output of the experiment: colours represent the amount of out-of-reference-plane displacement of the inflated specimen according to the scale reported on the right. (For interpretation of the references to colour in this figure legend, the reader is referred to the web version of this article.)
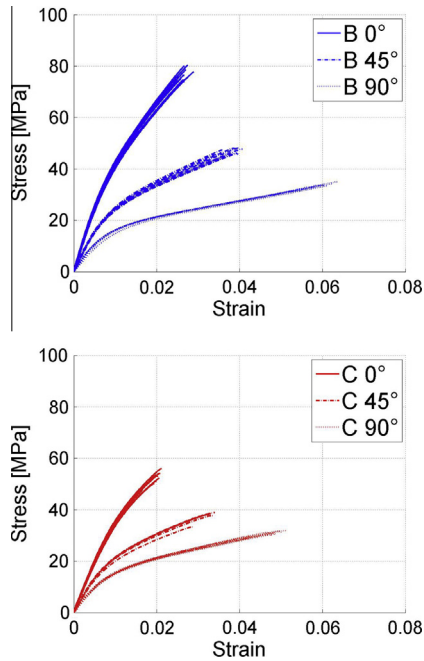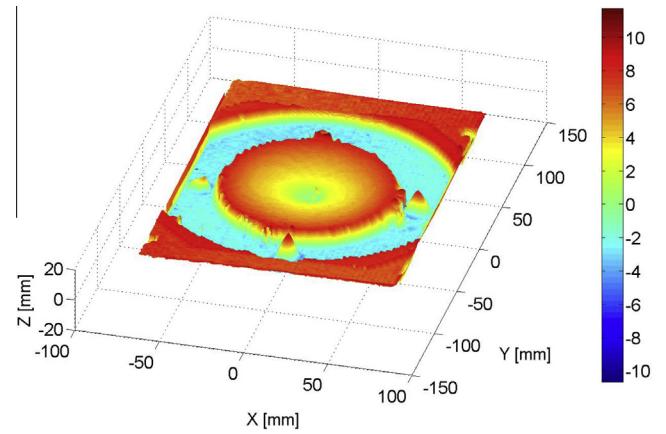
Fig. 1. Uniaxial stress–strain curves of specimens cut from two paperboard batches (named B and C) tested under displacement control along machine (0°), cross (90°) and diagonal (45°) direction.

laser blade profilometer connected to a computer monitors the out-of-plane displacements defining the geometry of the inflated membrane up to failure. A typical graphical output of the measurements performed during the experiment is represented in Fig. 3. It concerns the specimen shown in Fig. 4, which consists of the paperboard composite embedding a circular inclusion made of a polymer–aluminium laminate, usually situated in the cap opening area of beverage packages. The picture in Fig. 4 evidences the failure mode of this heterogeneous sample, which is induced by the sharp separation of the aluminium foil from the interface with the paperboard composite. This event occurs in a rather brittle fashion despite metals usually exhibit a ductile response. Nevertheless, pronounced size effects in thin laminated metal foils with significant reduction of toughness and fracture strain compared to the corresponding bulk have been observed already ([15,16]).

The unconventional results collected in the experimental campaign presented in this contribution are discussed at the light of
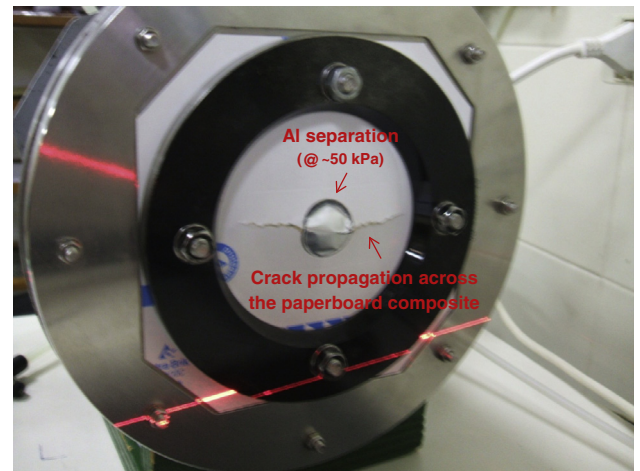

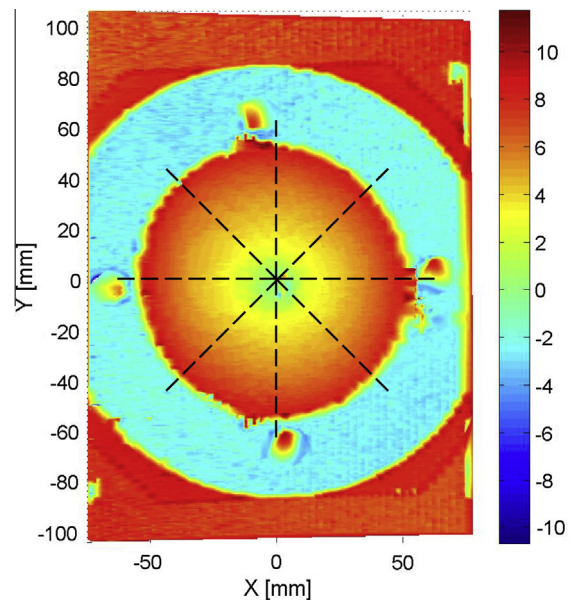Fig. 4. Failure mode of heterogeneous specimens.

Fig. 5. Graphical output of the inflation experiment: the colour map represents the amount of out-of-reference-plane displacement of an inflated specimen. (For interpretation of the references to colour in this figure legend, the reader is referred to the web version of this article.)
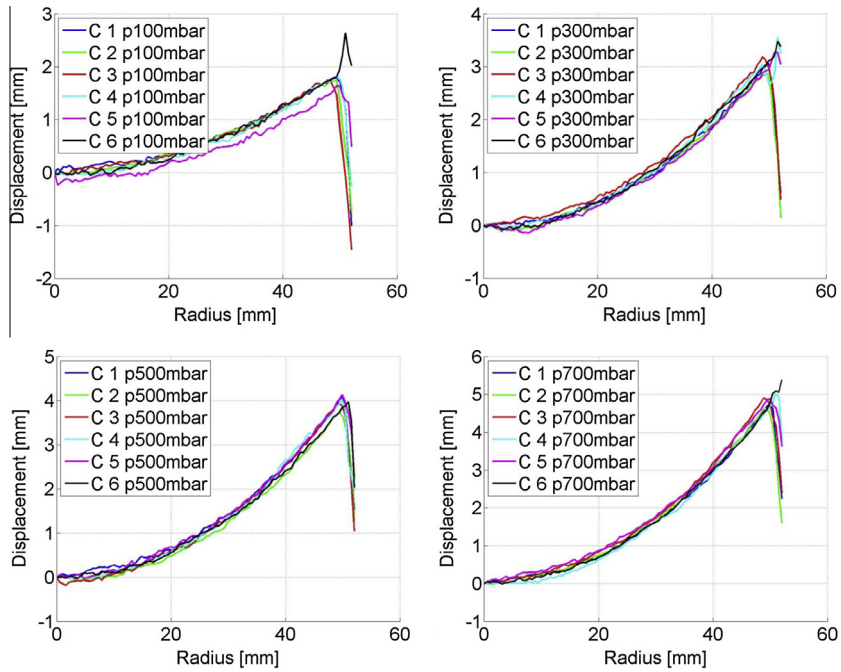

Fig. 2. The prototype equipment developed for controlled inflation tests: pressurized vessel (on the left) and monitoring system (on the right).

Fig. 6. Mean profiles of the inflated shape of six paperboard specimens tested at the pressure levels 100, 300, 500 and 700 mbar (i.e. 10, 30, 50 and 70 kPa).

the above observations and interpreted with the aid of validated numerical models of the performed tests.

The overall behaviour of the investigated material samples has been reproduced under the assumptions of orthotropic linear elasticity and associative plasticity obeying Hill's yielding criterion [17]. Similar hypotheses have been introduced to simulate paper folding and creasing, for instance in references [18–21]. These processes are dominated by inter-ply damage and delamination and therefore require a detailed description of the material composition. On the contrary, the macroscopic failure modes observed in the present investigation concern the overall response of the paperboard composite and of the aluminium laminate, which can be described by through-thickness homogenized models.

2. Testing procedure

The prototype instrumentation shown in Fig. 2 has been used to investigate the structural response of the considered composites under the loading condition more commonly experienced by beverage packaging, which engages all material directions contemporarily. The samples are placed over a circular hole of 50 mm radius opened on the top of the cylindrical vessel visualized on the left, filled with air at controlled pressure, temperature and humidity. The specimens are inserted between the stiff plates of an air-proof flange and fixed by the bolts shown by the pictures in Figs. 2 and 4. The out-of-plane displacements of the inflated membrane are monitored by the rotating laser-blade profilometer
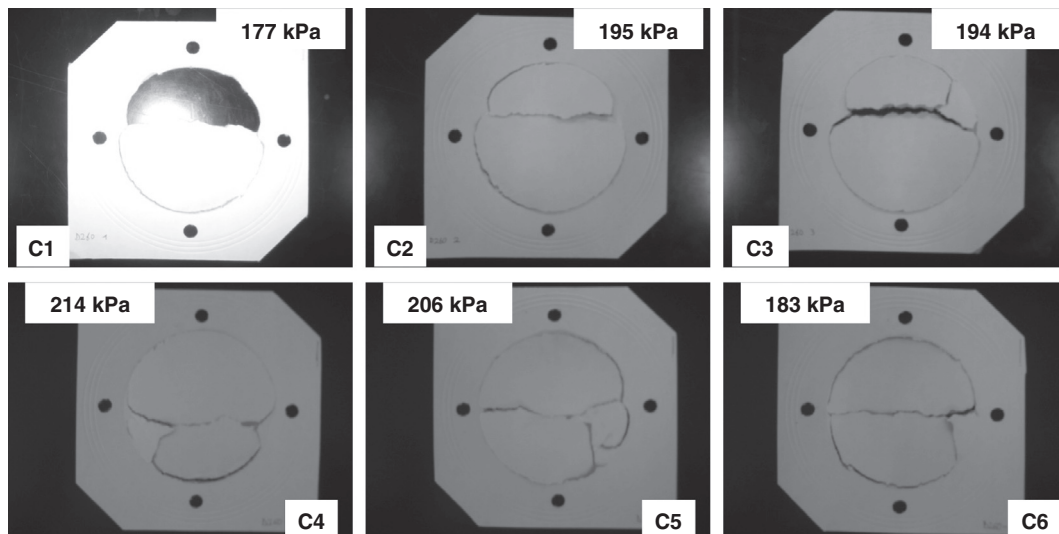

Fig. 7. Failure mode and corresponding pressure level of six specimens of material batch C (horizontal: cross direction; vertical: machine direction).

Table 1
Ultimate pressure levels of the paperboard material.

	Failure pressure (kPa)		
	Batch A	Batch B	Batch C
Specimen 1	185	171	177
Specimen 2	196	182	195
Specimen 3	179	175	194
Specimen 4	198	172	214
Specimen 5	181	176	206
Specimen 6	207	172	183
Average	191	175	195
Standard deviation	11	4	14

Table 2
Constitutive parameters entering Hill's material model calibrated on the basis of uniaxial tests performed on paperboard (1: cross direction; 2: machine direction).

	Batch A	Batch B	Batch C
E_1 (MPa)	2134	2154	1860
E_2 (MPa)	5150	4810	3646
G_{12} (MPa)	1336	1084	908
$R_{11}\sigma_0$ (MPa)	14.5	14.0	14.3
$R_{22}\sigma_0$ (MPa)	35.7	34.9	39.0
$R_{12}\sigma_0$ (MPa)	11.1	10.1	11.0
n (−)	0.41	0.45	0.48
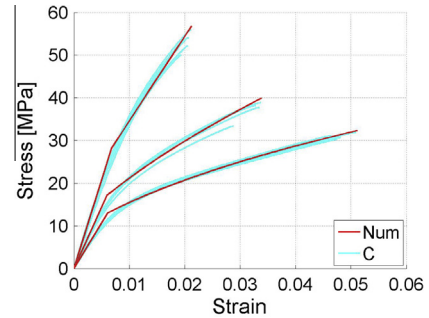
Fig. 9. Experimental results and calibrated stress–strain relationship for paperboard batch C.
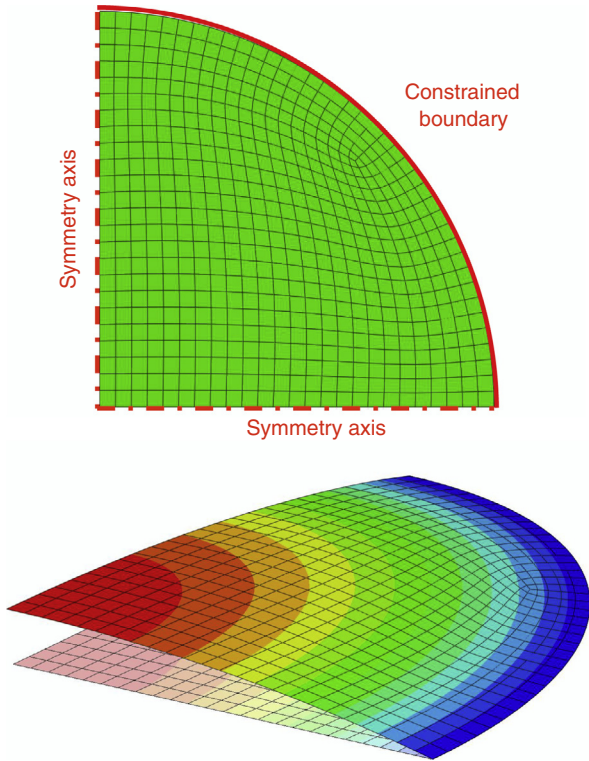

Fig. 8. Finite element simulation of the inflation test of paperboard; the colour map visualizes the almost axis-symmetric distribution of the out-of-plane displacements. (For interpretation of the references to colour in this figure legend, the reader is referred to the web version of this article.)

shown on the right of the picture in Fig. 2. Data acquired at pre-fixed load levels are transferred to a computer and stored for further use [12]. The pressure is increased of about 200 mbar/min (i.e. 20 kPa/min) up to failure.

The graphical representation of a typical output is shown in Fig. 3, which evidences the position of the fixing bolts. These rough data are returned in digital format and processed in order to transfer all information to an intrinsic reference system having two axes laying on a plane parallel to the initially flat membrane, easily individuated from the position of the plate supporting the flange. The third axis, orthogonal to this reference plane, crosses the membrane surface at its maximum inflation depth. The out-of-plane displacements of eight profiles, situated along radial directions at 45° one from the neighbouring others (see e.g. the dashed lines sketched in Fig. 5) are averaged.

The first performed experiments concerned plain paperboard. The mean inflated shape of 6 specimens extracted from the same batch are reported in Fig. 6 for the pressure levels 10, 30, 50 and 70 kPa (100, 300, 500 and 700 mbar). Notice the different scale

on the vertical axis of the graphs. The dispersion observed at the lower load levels is partly due to the natural corrugation of the paperboard foils, which is flattened by the traction generated in the membrane as the pressure increases.

Under this uniform loading condition, the failure of the paperboard foils is systematically induced by a main crack, which propagates quickly in the direction orthogonal to the stiffest and strongest machine direction (MD), see Fig. 7. The ultimate pressure levels are listed Table 1. For each material batch, the standard deviation observed over the six tested samples is at most 7% of the corresponding average value (between 175 and 195 kPa).

The inflation test can be exploited to investigate the more complex material system visualized in Fig. 4, typical of the cap opening area of beverage packages. In this case, a polymer–aluminium laminate inclusion is embedded in the paperboard composite. Under uniform pressure, failure is initiated by the separation of the aluminium foil from the paperboard composite at the boundary between the two dissimilar media. Then, two almost parallel cracks propagate quickly across the central portion of the specimen, as illustrated by Fig. 4, at much lower pressure (about 50 kPa) than that supported by the plain paperboard samples. Eventually, the elastic energy liberated in this bursting process let fracture cross the aluminium inclusion.

These experimental results have been interpreted at the light of the numerical simulation of the tests, performed by the finite element models illustrated in the next Section.

3. Numerical simulation

The experiments performed during this study and concerning either the plain paperboard or the paperboard composite were reproduced by finite element (FE) models (shown for instance in Fig. 8). The considered constitutive relationships reflect the homogenized material response, that can be described by orthotropic linear elasticity and Hill's plasticity model [17]. Since both uniaxial and inflation tests produce essentially membrane stress state
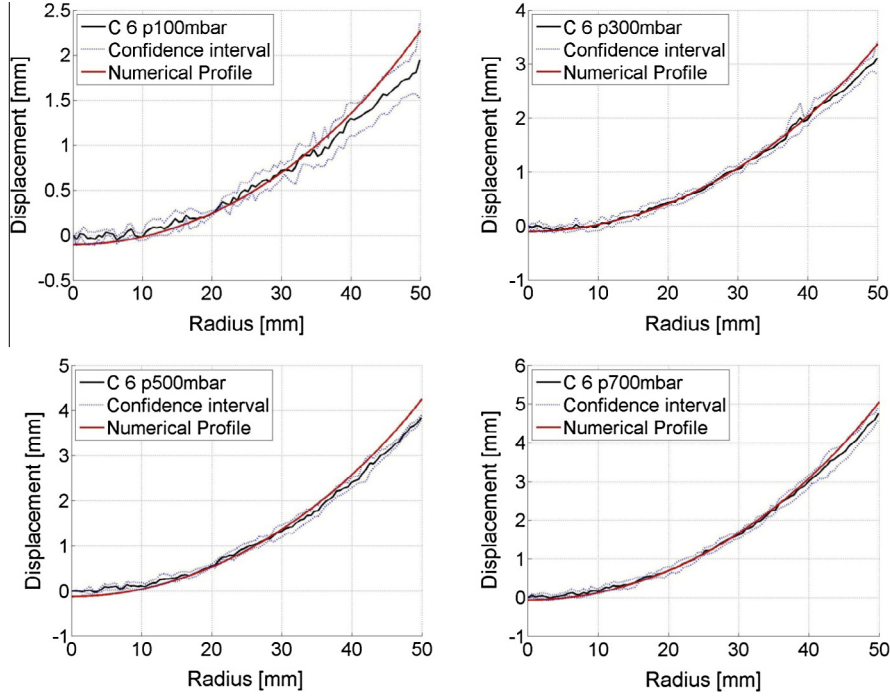
Fig. 10. Comparison between experimental and numerical results of the inflation test: average profile of the inflated membrane in the case of a paperboard specimen under pressure values 10, 30, 50 and 70 kPa (corresponding to 100, 300, 500 and 700 mbar).

in the material specimens, the formulation can be referred to a local reference system coinciding with the in-plane material symmetry axes, here named 1 and 2, and with the thickness direction 3.

In this context, the relationship between the most meaningful components of the strain and stress tensors ($\underline{\varepsilon}$ and $\underline{\sigma}$, respectively) can be expressed in the elastic range by the relationship:

$$\begin{Bmatrix} \varepsilon_{11} \\ \varepsilon_{22} \\ \gamma_{12} \end{Bmatrix} = \begin{bmatrix} 1/E_1 & -v_{21}/E_2 & 0 \\ -v_{12}/E_1 & 1/E_2 & 0 \\ 0 & 0 & 1/G_{12} \end{bmatrix} \begin{Bmatrix} \sigma_{11} \\ \sigma_{22} \\ \sigma_{12} \end{Bmatrix} \tag{1}$$

The symmetry of the constitutive matrix introduced in (1) requires that the ratio v_{21}/v_{12} between the lateral contraction ratios equals the ratio between the moduli E_2/E_1.

The elastic threshold is defined in terms of Hill's equivalent stress, namely:

$$\sigma_{eq} = \sqrt{\left(\frac{\sigma_{11}}{R_{11}}\right)^2 + \left(\frac{\sigma_{22}}{R_{22}}\right)^2 - \left(\frac{1}{R_{11}^2} + \frac{1}{R_{22}^2} - \frac{1}{R_{33}^2}\right)\sigma_{11}\sigma_{22} + \left(\frac{\sigma_{12}}{R_{12}}\right)^2} \tag{2}$$

where R_{11}, R_{22}, R_{33} and R_{12} define the ellipsoidal shape of the elastic domain, governed by the initial yield limits $\sigma_{11}^Y = R_{11}\sigma_0$, $\sigma_{22}^Y = R_{22}\sigma_0$ and $\sigma_{33}^Y = R_{33}\sigma_0$ along the main material directions and by the shear yield stress $\sigma_{12}^Y = R_{12}\sigma_0$.

Under the loading conditions considered in this contribution, irreversible deformation starts developing as σ_{eq} assumes the reference value σ_0 and then increases progressively.

An equivalent scalar measure of the plastic strain can be introduced, assuming that the work associated to the plastic strain increment $\delta\underline{\varepsilon}^p$ can be expressed by the product $\sigma_{eq}\delta\varepsilon_{eq}^p$. This equivalence leads to the definition of ε_{eq}^p through a quadratic form analogous to (2), with coefficients derived from the above introduced factors R_{ij} ($i, j = 1,3$) [22]. Details on this classical formulation and on its numerical implementation can be found for instance in [23].

Beyond the elastic threshold, the equivalent stress measure σ_{eq} attains a limiting value that evolves with the deformation ε_{eq}^p

accumulated during the plastic process. This dependence is here described by the exponential hardening rule:

$$\sigma_{eq} = \sigma_0 \left(1 + \frac{\varepsilon_{eq}^p}{\varepsilon_0}\right)^n \tag{3}$$

where the normalization factor ε_0 is assumed to coincide with the ratio σ_{11}^Y/E_{11}.

The equivalent stress σ_{eq} and the corresponding plastic strain measure ε_{eq}^p reduce to those corresponding to the classical Hencky–Huber–von Mises (HHM) formulation for isotropic solids when $R_{11} = R_{22} = R_{33} = 1$ and $R_{12} = 1/\sqrt{3}$. This particular assumption is suitable to describe the threshold of the irreversible deformation developing in the aluminium–polymer laminate [24]. The amount of σ_{eq} during plastic flow is defined in this case by an hardening rule with saturation stress, namely:

$$\sigma_{eq} = \sigma_0 + \sigma_1(1 - e^{-N\varepsilon_{eq}^p}) \tag{4}$$

where the reference value σ_0 coincides with the initial yield limit and the parameter σ_1 represents the maximum strength increase, which is asymptotically reached for large values of the equivalent plastic strain (theoretically, for $\varepsilon_{eq}^p \to \infty$).

The above introduced constitutive models have been associated to the FE discretization of the experimentally investigated foils visualized for instance in Fig. 8. The analyses have been performed in the large displacement regime in order to overcome the initial hypostatic condition of the flat pressurized membrane. A commercial code [25] often exploited for paperboard simulations (e.g. [3,11,18,21]) has been used. Both 4-node membrane and 4-node homogeneous shell elements based on Mindlin–Reissner flexural theory have been considered to modelling purposes. Since specific information on the out-of-plane characteristics of the foils was not available, the same value of the shear modulus G_{12} was assumed also for G_{13} and G_{23} as previously done, for instance in [18]. This rough approximation (see e.g. [7,20]) overestimates the shear stiffness and, hence, enhances the load carrying capability of the model by flexural contributions. Nevertheless, differences in the results were insignificant. In fact, the ratio between the characteristic size
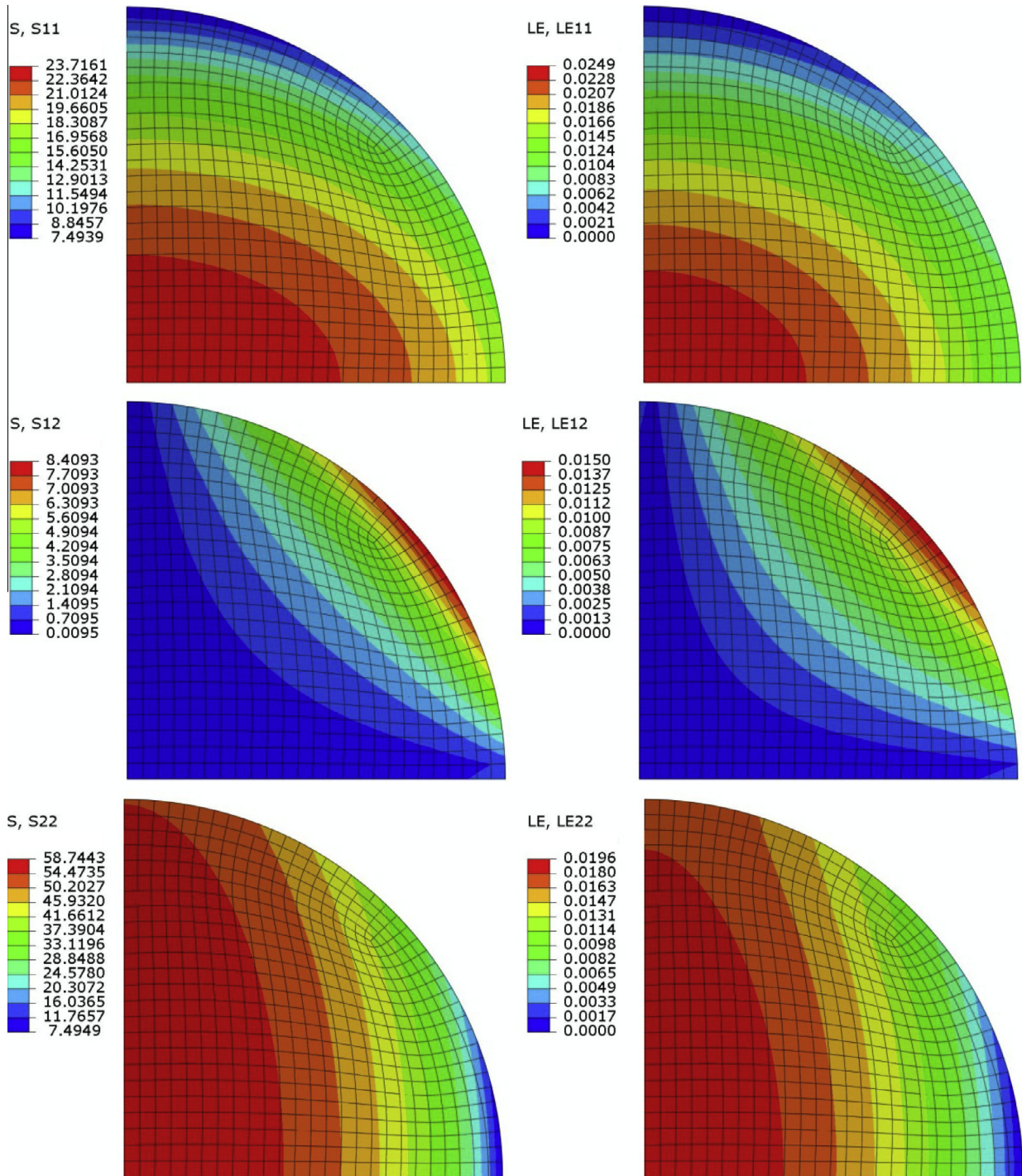
Fig. 11. Stress and strain distribution at about the failure pressure (190 kPa) of batch C specimens (1 – horizontal: cross direction; 2 – vertical: machine direction).

of the pressurized surface (50 mm radius) and the thickness of the sampled specimens (indicatively: 0.4 mm for plain paperboard; 0.5 mm for the paperboard composite) is extremely reduced. The same holds true also for the circular inclusion visualized in Fig. 4, with 12.5 mm radius, 0.1 mm thickness.

4. Model validation and identification of the failure mode

The constitutive parameters entering relationships (1) and (2) have been calibrated on the basis of the output of tensile tests

performed on material strips according to Standards [2]. The results represented for instance in Fig. 1 concern the case of plain paperboard. CD is denoted as direction 1 in the modelling, MD coincides with direction 2 and direction 3 is orthogonal to the foil surface.

Parameter R_{33} was set equal to R_{11}, a quite common assumption of creasing and folding simulations of paperboard ([18–21]). This simplification is particularly justified in the present context also in view of the reduced sensitivity of the in-plane material response to the through-thickness strength, evidenced already in a former study concerning the inflation test [11]. The marginal role of the
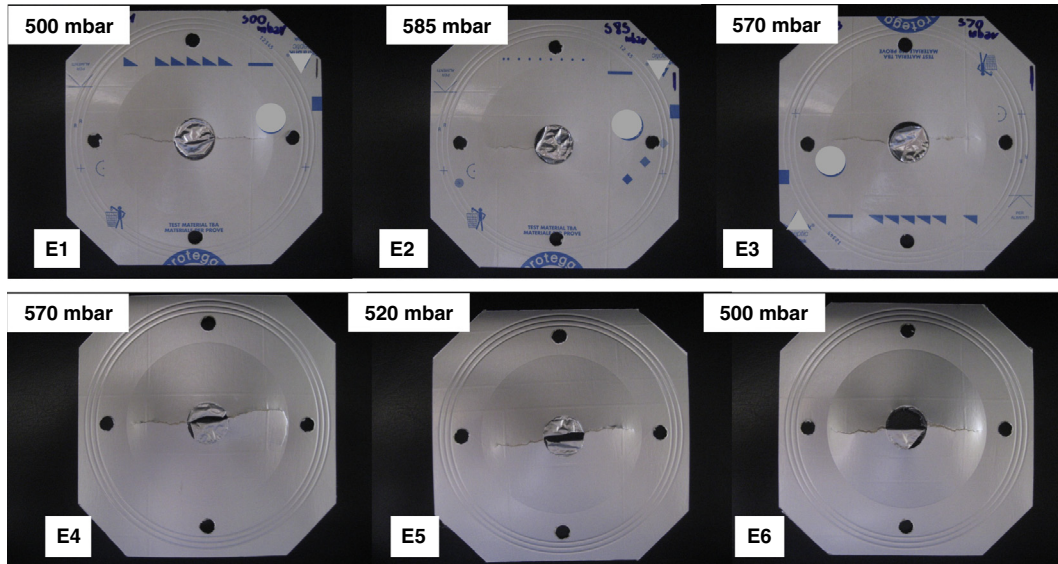
Fig. 12. Failure mode and corresponding pressure level of six heterogeneous material samples (horizontal: cross direction; vertical: machine direction).
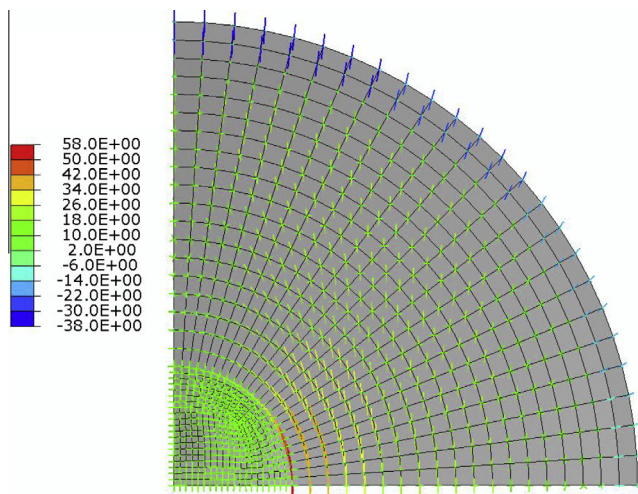

Fig. 13. Principal stress distribution in the inflated heterogeneous specimen at 50 kPa (500 mbar) applied pressure.

coefficient associated to the stress coupling term $\sigma_{11}\sigma_{22}$ in relation (2) is confirmed also by the analysis of several failure criteria and numerous sets of experimental data recovered from bi-axial testing of paperboard [9].

Table 2 lists the elastic moduli E_1, E_2 and G_{12}, the initial yield limits $R_{11}\sigma_0$, $R_{22}\sigma_0$, $R_{12}\sigma_0$ and the hardening exponent n of the investigated paperboard batches. Parameters were not recovered one by one, but their optimal value was identified from the best overall fitting of the tensile curves. The resulting approximation of the real material response can be appreciated from the graphs drawn in Fig. 9, concerning the representative case of material C.

The lateral contraction coefficient v_{12} was set equal to the value 0.2 in all considered situations while v_{21} values were recovered from the symmetry of the elastic constitutive matrix introduced in (1) in the quite typical literature range 0.39 (batch C)–0.48 (batch A), see e.g. [3,18,20].

The reliability of the so calibrated constitutive models can be assessed on the basis of the measurements performed during the inflation test, summarized in terms of mean values and of the relevant confidence interval by the graphs in Fig. 10 for batch C. The experimental information is compared with the output of the
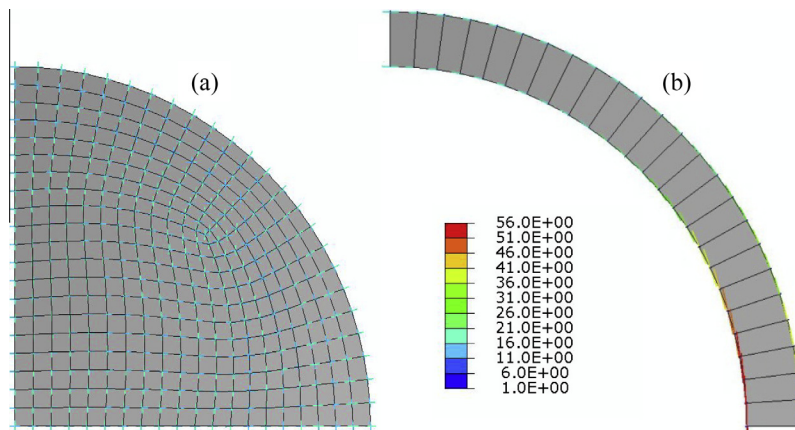

Fig. 14. Principal stress distribution at 50 kPa (500 mbar) applied pressure in the polymer–aluminium laminate (a) and in the paperboard composite close to the boundary with the internal inclusion (b).
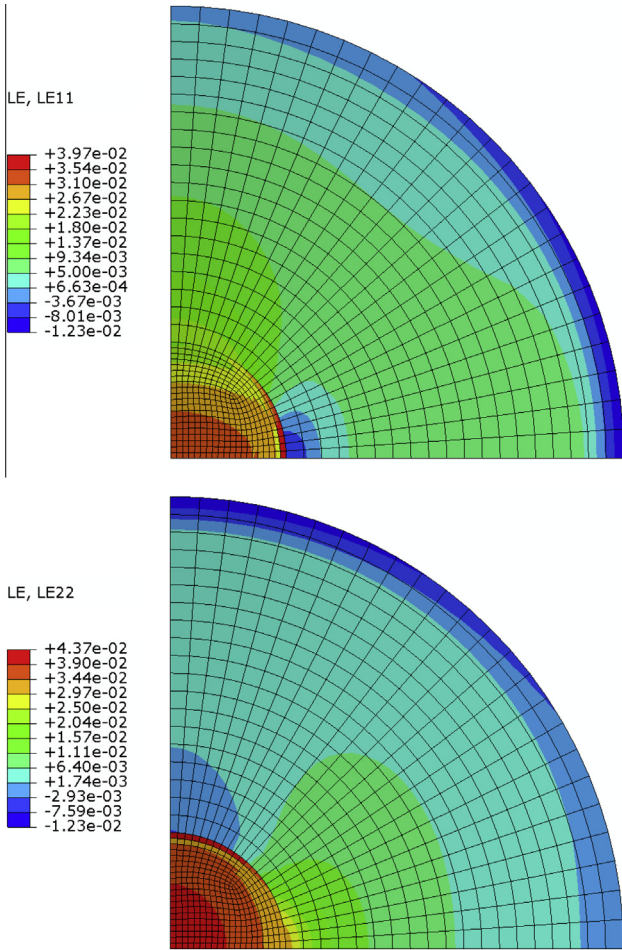
Fig. 15. Colour map of the strain distribution in the inflated heterogeneous specimen at 50 kPa (500 mbar) applied pressure (1 – horizontal: cross direction; 2 – vertical: machine direction). Labels indicate the extreme values in the sample. (For interpretation of the references to colour in this figure legend, the reader is referred to the web version of this article.)

numerical simulation. The agreement between the measured and the computed displacement distribution is always fairly good. Accuracy increases with the pressure level, where non-linearity dominates the material response and measurement noises are reduced.

FE results show that the marked anisotropy evidenced by the uniaxial tests is not reflected by the geometry of the inflated membrane, which does not differ significantly from the axis-symmetric response of isotropic foils, see e.g. the colour map of Fig. 8. On the contrary, anisotropy affects the stress and strain distribution, represented in Fig. 11 at about the failure pressure of batch C specimens. In this situation, stress and strain components aligned with the stiff MD reach values comparable to the material strength and to the corresponding elongation in uniaxial test (about 55 MPa maximum stress and 2% maximum strain), while in the orthogonal direction (CD) resistance is not yet exhausted.

These preliminary results help understanding the collapse mode of the heterogeneous material specimens, visualized in Fig. 12. In this configuration, failure induced by the applied pressure is initiated by the separation of the aluminium foil from the paperboard composite at the interface between the two dissimilar media at about 50 kPa (500 mbar), a much lower value than plain paperboard. Detaching starts from an almost random position and propagates toward the diameter of the sample, which is aligned

E_1 (MPa)	E_2 (MPa)	G_{12} (MPa)	$R_{11}\sigma_0$ (MPa)	$R_{22}\sigma_0$ (MPa)	$R_{12}\sigma_0$ (MPa)	n (–)
1711	3015	693	10.6	31.0	8.9	0.41

with CD. The polymer films, still undamaged, bear the pressure until two cracks emanate from the interface between the aluminium laminate inclusion and the surrounding material and propagate in the paperboard composite toward the external specimen boundary in a fast, almost symmetrical and rather catastrophic manner.

The inflation process of the heterogeneous material samples has been simulated by the FE discretization visualized in the graphs of Figs. 13–15. The behaviour of the polymer–aluminium laminate inclusion, characterized in earlier performed investigations [24], is interpreted by HHM plasticity with the saturation hardening rule (4). The assumed values of the constitutive parameters are: $E = 3150$ MPa; $v = 0.3$; $\sigma_0 = 5.45$ MPa; $\sigma_1 = 12.50$ MPa; $N = 34.5$. Hill's constitutive model and exponential hardening rule (3) describe the mechanical response of the paperboard composite. The material characteristics, listed in Table 3, have been calibrated on the basis of the data collected from tensile tests performed on material strips cut along CD and MD, see Fig. 16. The worth noting similarity between the graphs reported in Figs. 16 and 9 has been exploited to define the shear properties.

Fig. 17 visualizes the average radial profiles of the inflated heterogeneous membrane, detected by laser scan at different pressure levels. The corresponding scatter is also represented. Larger experimental noise is manifested in comparison to the formerly investigated situations due to reflectiveness of the bright surfaces span by the laser blade. The presence of the compliant internal inclusion is progressively evidenced as the pressure increases. The graphs show that the experimental results compare well with the output of the numerical simulation also in this case.

The principal stress distribution in the heterogeneous composite sample, computed by the validated model at 50 kPa applied pressure (close to failure), is displayed in Figs. 13 and 14. Stresses are almost homogeneous and equi-biaxial in the isotropic polymer–aluminium laminate despite the slight geometrical ovalization produced by the strongly anisotropic surrounding material, see Fig. 15. The output of this simulation show that the aluminium detaching process occurs at about 4% material elongation, with stress values corresponding to the material strength ($\sigma_0 + \sigma_1$) exhibited by the laminate under uniaxial tensile test. This result is consistent with the findings of earlier investigations carried out in free standing thin (20–300 μm) metal foils, evidencing
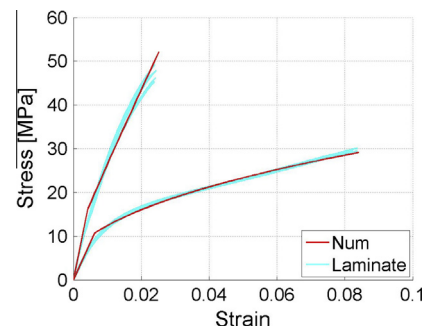

Fig. 16. Experimental results and calibrated nominal stress vs. nominal strain relationship for the paperboard composite.
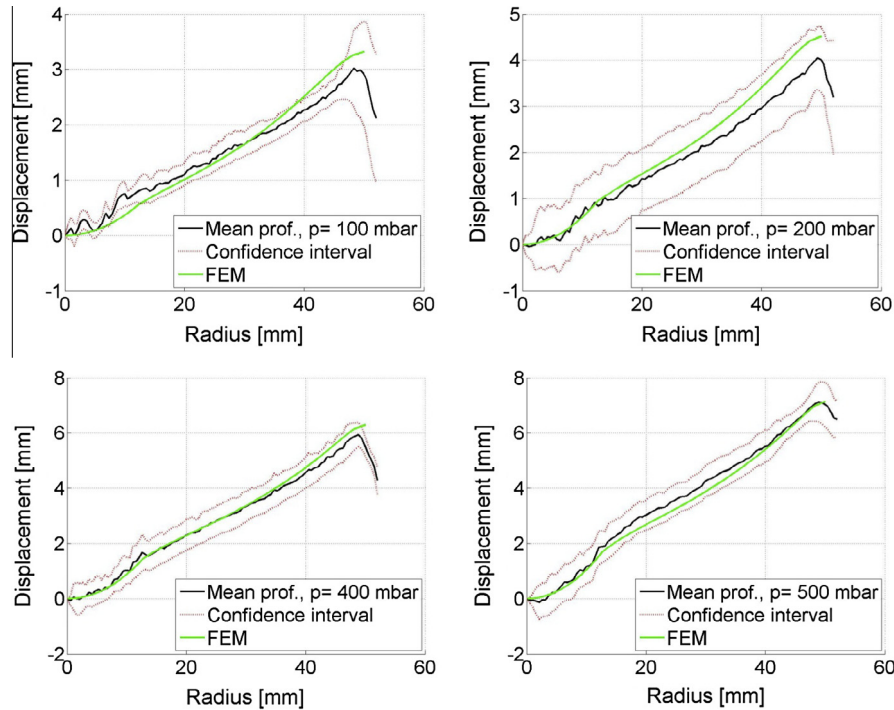
Fig. 17. Comparison between experimental and numerical results of the inflation test: average profile of the inflated membrane in the case of the heterogeneous material specimen under pressure values 10, 20, 40 and 50 kPa (corresponding to 100, 200, 400 and 500 mbar).

meaningful reduction of toughness and fracture strain with the thickness decrease below some threshold ([15,16]). The present study concerns thinner (6–9 μm) metal layers and evidences that similar effects are not prevented by the coupling with relatively thick (70–100 μm) polymer coatings.

Graph (b) in Fig. 14 shows that stresses become circumferential in the area of the paperboard composite close to the boundary between the two dissimilar media. The compliance of the internal inclusion induces stress concentration and a steep stress gradient in the surrounding material, especially along the diameter aligned with CD, see e.g. Fig. 13. The magnitude of the stress parallel to MD is comparable with the overall strength of the composite. The maximum computed stress at the interface (54 MPa) slightly exceeds the resistance exhibited by the material in uniaxial test (about 50 MPa), but the average stress value evaluated over the length aligned with CD of the first FE amounts to about 38 MPa, evidencing the possibility of some marginal redistribution. Thus cracks propagate across the paperboard toward the external boundary of the sample when the aluminium layer is mostly detached and no longer contributes to the load carrying capacity of the specimen.

5. Closing remarks

Homogeneous paperboard specimens and heterogeneous composite samples have been subjected to traditional tensile tests and to non-conventional inflation experiments, carried out by a prototype instrumentation inspired by burst strength testers for papers and supplied with a laser monitoring system, which permits to follow the geometry change of the inflated membrane during the test.

The equipment applies uniform pressure to the foil surface, thus failure is not influenced by the loading direction but governed by the material characteristics.

The collected experimental information has been interpreted with the aid of a validated numerical model of the performed tests. The mechanical response of the investigated material systems was described by linear elasticity and Hill's plasticity with isotropic hardening rule, with constitutive parameters calibrated on the output of uniaxial tensile tests. The independent results gathered from the inflation tests were used to verification purposes. The displacement distribution defining the deformed geometry of the pressurized membranes were accurately predicted without any adjustment.

Simulations helped understanding that the collapse mechanisms of the considered material samples is dominated by brittle fracture. The unstable nature of crack propagation through paperboard has been confirmed by recently published results. The present investigation shows that this feature is transferred to the paperboard composites that constitute common beverage packaging.

The rather brittle characteristics of the thin (6–9 μm) aluminium layer embedded in this functional material were also evidenced by the performed tests. Similar published results concerned free standing metal foils of minimum thickness 20 μm.

References

[1] ISO 534:2011 Paper and board – Determination of thickness, density and specific volume.
[2] ISO 1924-2:2008 Paper and board – Determination of tensile properties – Part 2: Constant rate of elongation method (20 mm/min).
[3] Mäkela P, Östlund S. Cohesive crack modelling of thin sheet material exhibiting anisotropy, plasticity and large-scale damage evolution. Eng Frac Mech 2012;79:50–60.

[4] Xia QS, Boyce MC, Parks DM. A constitutive model for the anisotropic elastic–plastic deformation of paper and paperboard. Int J Solids Struct 2002;39:4053–71.

[5] Castro J, Ostoja-Starzewski MO. Elasto-plasticity of paper. Int J Plast 2003;19:2083–98.

[6] Makela P, Ostlund S. Orthotropic elastic–plastic material model for paper materials. Int J Solids Struct 2003;40:5599–620.

[7] Harrysson A, Ristinmaa M. Large strain elasto–plastic model of paper and corrugated board. Int J Solids Struct 2008;45:3334–52.

[8] Nygårds M. Experimental techniques for characterization of elastic plastic material properties in paperboard. Nordic Pulp Paper Res J 2008;23:432–7.

[9] Suhling JC, Rowlands RE, Johnson MW, Gunderson DE. Tensorial strength analysis of paperboard. Exp Mech 1985;25:75–84.

[10] Lim W-K, Jeong W-K, Tschegg EK. Failure of fibrous anisotropic materials under combined loading. Composites B 2010;41:94–7.

[11] Ageno M, Bolzon G, Maier G. An inverse analysis procedure for the material parameter identification of elastic–plastic free-standing foils. Struct Multidisc Optim 2009;38:229–43.

[12] Ageno M, Bocciolone M, Bolzon G, Cigada A, Maier G, Zappa E. Mechanical characterisation of thin foils by profilometer measurements of inflated membranes. In: Proceedings of the 12th international conference on experimental mechanics, ICEM12, Bari, Italy, August 29–September 2; 2004.

[13] ISO 2758: 2001 Paper – determination of bursting strength.

[14] Galliot C, Luchsinger RH. Uniaxial and biaxial mechanical properties of ETFE foils. Polym Test 2011;30:356–65.

[15] Hadrboletz A, Weiss B, Khatibi G. Fatigue and fracture properties of thin metallic foils. Int J Fract 2001;107:307–27.

[16] Wang HW, Kang YL, Zhang ZF, Qin QH. Size effect on the fracture toughness of metallic foil. Int J Fract 2003;123:177–85.

[17] Hill R. A theory of the yielding and plastic flow of anisotropic materials. Proc R Soc Lond A 1948;193:281–97.

[18] Barbier C, Larsson PL, Östlund S. Numerical investigation of folding of coated papers. Compos Struct 2005;67:383–94.

[19] Thakkar BK, Gooren LGJ, Peerlings RHJ, Geers MGD. Experimental and numerical investigation of creasing in corrugated paperboard. Phil Mag 2008;28–29:3299–310.

[20] Beex LAA, Peerlings RHJ. An experimental and computational study of laminated paperboard creasing and folding. Int J Solids Struct 2009;46:4192–207.

[21] Huang H, Hagman A, Nygårds M. Quasi static analysis of creasing and folding for three paperboards. Mech Mat 2014;69:11–34.

[22] Bolzon G, Talassi M. An effective inverse analysis tool for parameter identification of anisotropic material models. Int J Mech Sci 2013;77:130–44.

[23] De Borst R, Feenstra PH. Studies in anisotropic plasticity with reference to the Hill criterion. Int J Num Meth Eng 1990;29:315–36.

[24] Bolzon G, Buljak V, Zappa E. Characterization of fracture properties of thin aluminium inclusions embedded in anisotropic laminate composites. Fract Int Struct 2012;19:20–8.

[25] ABAQUS/Standard, Theory and user's manuals, release 610-1. Pawtucket, RI, USA, HKS Inc. 2010.